IET Renewable Power Generation

Research Article

Proof of concept for a novel and smart shade resilient photovoltaic module

ISSN 1752-1416
Received on 13th November 2018
Revised 10th April 2019
Accepted on 21st May 2019
E-First on 5th July 2019
doi: 10.1049/iet-rpg.2018.6127
www.ietdl.org

Sayedeh Zahra Mirbagheri Golroodbari[1] ✉, Anne Celeste de Waal[1], Wilfried G.J.H.M. van Sark[1]

[1]*Copernicus Institute of Sustainable Development, Utrecht University, Vening Meinesz building, Princetonlaan 8a, 3584 CB Utrecht, The Netherlands*

✉ *E-mail: s.z.mirbagherigolroodbari@uu.nl*

Abstract: In this study, the performance of a shade resilient smart module is studied under a dynamic shading pattern. A smart module architecture is developed to mitigate the non-linear shading effect on the module performance. Partial shading decreases the output current of the shaded cells and affects the unshaded cells' output power. After distributing the module cells into small groups, based on a least square support vector machine optimisation method, DC–DC buck converters compensate the decreased current levels, by adjusting the output current and voltage level from any individual group of cells. The system is simulated in the MATLAB Simulink environment, and the output results are presented. Results show that the module performs efficiently and output power of the unshaded groups of cells never decreased because of the effect of shading on the other groups. Additionally, the maximum output power is harvested from all groups simultaneously. Prototype hardware is designed and built to implement the proof of concept. The real-time results of hardware testing show that the smart module performs as expected and mitigates partially shaded conditions by extracting maximum power from each group, regardless of other groups shading condition.

1 Introduction

Every year the solar industry is breaking new records, e.g. the global photovoltaic (PV) market grew significantly to at least 74.4 GW in 2016 [1]. In the year 2017, 29 countries exceeded the gigawatt (GW) mark, and as a result, the global PV market rose for the first time to at least 98 GW, which is >32% increase in a year [2]. However, analysis of energy yields reveals that the optimum performance is not always obtained, and it is affected by the ambient conditions, and shading is a prominent cause of performance loss [3]. Thus, to harvest energy from a PV module, proper maximum power point tracking (MPPT) is needed, as well as DC to AC conversion. Minimising the effects of shading on modules has been proposed by several authors such as by using complicated MPPT algorithms, dynamic reconfiguration (DR) methods, voltage equalisers, etc. [4–8].

As an interface between module and load, an MPPT is implemented to both control and maximise the output PV power via an MPPT algorithm. A significant number of MPPT algorithms have been presented in the literature, which can mainly be categorised into three different groups: (i) 'Quasi seeking' known as offline methods, which depend on the physical aspects of the module and mathematical models, e.g. curve-fitting, open-circuit voltage or short-circuit current methods [9, 10]; (ii) 'True seeking' also called online methods, which are based on measured data from the panel. Most of the conventional MPPT algorithms which are basically gradient descent based and also denoted as hill climbing algorithms are classified into these groups, e.g. perturb and observe (P&O) and incremental conductance (Inc. Cond) [11–13]; (iii) Hybrid methods which are either categorised as a combination of online and offline methods [14–16] or are responsible for both MPP tracking and output voltage controlling [17, 18].

It is indicated in many studies that conventional MPPT methods perform much better under non-shaded conditions, and other methods are either imprecise or knotty [14, 15]. A concave power–voltage ($P-V$) curve as a characteristic specification of a PV module could be changed due to the performance of bypass diodes (BPDs) in mismatch conditions (MC). The non-linear effect of MC changes the $P-V$ curve to a cluster of concave curves; as a result, instead of only one maximum, the $P-V$ curve has several local maxima and only one global maximum (GM). One may say that a solution to mitigate MC effects, is to equip every single cell with one BPD, while we noted that although more BPDs lead to shade-resilient modules [19], first, the consequential efficiency losses with the BPDs should be considered and also, the number of BPDs has a direct relation with the number of local maxima [6]. It is indicated in many reports that the conventional MPPT methods may fail to find the GM or recognise the first local maximum instead of that [14, 15]. To mitigate the MC or partial shading condition (PSC) researchers either developed the conventional methods [20, 21] or frequently turned to implement AI, e.g. evolutionary algorithms (EAs), fuzzy logic (FL) methods, genetic algorithm (GA), particle swarm optimisation (PSO), etc. Aside from the complexity of AI methods, it can be concluded that the non-linear effect caused by MC, will either decrease the efficiency and accuracy of the MPPT algorithms or give a sluggish performance [14, 22].

An alternative solution for the non-linear effect of MC is to change the PV configuration, which is known as dynamic reconfiguration (DR) [8]. These methods, mostly implemented on the module level, clearly utilise an optimisation algorithm. These algorithms are to find the optimum configuration to mitigate shading effects by choosing between (i) series–parallel (SP); (ii) total-cross-tied (TCT); and (iii) bridge-linked module connection schemes and may be very complicated and markedly slow [5, 23].

Another alternative for mitigation of non-linear MC effect is called distributed MPPT (DMPPT), where first divided the cells in the module into smaller groups of cells and then instead of using a passive BPD implement an active BPD for each group of cells. An active BPD is an electrical circuit consisting of metal-oxide-semiconductor field-effect transistors (MOSFETs), which could be controlled via a duty cycle as the control signal. Such a configuration from now on is referred to as module integrated electronics (MIE) in this work. MIEs can implement either (i) a buck converter, (ii) a buck–boost converter, or (iii) a voltage equaliser [6, 24]. In conventional modules, the cells are divided into some groups (mainly three) of series connected cells and each group comes equipped with one BPD; then, the module supplies power to the MPPT converter, and the MPPT algorithm optimises the amount of harvested energy. MIEs using buck or buck–boost

Table 1 Specifications for one cell

V_{MPP}	I_{MPP}	V_{OC}	I_{SC}	FF	Efficiency (η)
0.49 V	7.54 A	0.61 V	7.92 V	0.765	16.4%

Table 2 LTM4611 specifications

$V_{in_{min}}$	$V_{in_{max}}$	$V_{out_{min}}$	$V_{out_{max}}$	$I_{out_{max}}$	SF[a]
1.5 V	5.5 V	0.8 V	5 V	15 V	835 Hz

[a]Switching frequency.

converters are potential interest to control current or voltage and current of the shaded group. Voltage equalisers, which are a combination of different converters or even bidirectional converters to equalise the voltage by power processing.

In the literature, there are several number of MPPT algorithms developed by researchers to maximise the harvested energy from the PV system. In [25], to track the MPP, the PV module instantaneous power is compared to a varying power reference generating by the MPPT algorithm. The algorithm is based on a two-loop control approach. The inner loop uses a sliding-mode strategy, and the outer loop is based on the MPPT algorithm generating the appropriate value of the static conductance required by the inner loop. However, because of the following reasons this method is not recommended for a small group of cells: (i) the complexity of this method making the tracking time long and (ii) the voluminous electronics circuits makes it impossible to mount it at the junction box. The researchers in [26] propose a PSO-based MPPT algorithm for dynamic environmental conditions. However, the simplicity and pace of algorithm are very important for a system with a few number of cells and low voltage level.

There are quite a number of studies on DMPPT in published papers. In [27], single-switch voltage equalisers using multi-stacked buck–boost converters are implementing to mitigate the MC issues. The proposed voltage equalisers can be derived by stacking capacitor–inductor–diode (CLD) filters on the traditional buck–boost converters, such as SEPIC, Zeta, and Ćuk converters. Although this technique is easy to install as it does not need local sensors and communication system, but it does not guarantee that all solar modules or cells perform at MPP. To make sure that the technique can both mitigates the MC and also performs at MPP, in [28] a distributed PV system architecture is proposed, the system requires one sensor, and the SS-MPPT method is implemented for this architecture [29]. The authors develop a new architecture to reduce the cost for the system, but the complexity of the system and the relatively slow MPPT algorithm are the drawbacks of this method.

In this paper, we employ the method for mitigating the partial shading condition as one of the most frequent mismatch and performance loss conditions. The main idea is to design a panel consisting of several groups of cells, such that each group is equipped with one individual micro-converter for the MPPT algorithm. The novelty in this research is that this method is in the panel order and the final control circuit is small enough to be mounted at the back of the panel in the junction box. Thus smart panel can be a more efficient replacement for the conventional panel. The smart panel can be implemented standalone or grid-connected, e.g. on the roof tops or facades for the building-integrated PVs (BIPVs) systems.

The smart module in this study is an MIE, which is designed as follows. First, a least square support vector machine (LS-SVM) algorithm is used to optimise the number of cells per group, a generic study on this optimisation and design and also, annual analysis with real data for the year 2016 with different shading pattern is published in [23]. Each group of cell supplies power to a micro-converter which is controlled using a sampling-based MPPT algorithm (Sweep Method MPPT (SM-MPPT)). This algorithm implements two main functions, *SubGradients* and $find(D_{max})$, to maximise the harvested energy. The *SubGradients* function is implemented to recognise the change either in temperature or irradiation level, which can cause the output power to vary. The $find(D_{max})$ is a sampling function which accurately finds the optimum duty cycle for the selected group of cells. Because of the system topology, the output current flow in all converters is equal as all converters are in series in their outputs. This strategy extracts as much power as each group of the cell could generate, even though some groups may be very heavily shaded. The conventional system bypasses the shaded groups because of the implemented BPDs, but in the smart module architecture, all cells, even shaded ones, are producing power efficiently, and none of the cells is bypassed.

In this study, we will discuss in details about the topology, MPPT algorithm, and electronics circuit design of the system. To investigate the feasibility of the smart module, the MATLAB/SIMULINK environment is used to simulate the module and to test both its MPPT time and accuracy. Also, a hardware prototype is built as a proof of concept. The prototype shows (i) how energy harvesting from each group individually is possible, (ii) how each group of cells could follow the irradiation change, (iii) to find the maximum power regardless of the connected load. The hardware is tested under a partial shading condition and data from all groups of cells is recorded.

This paper is organised as follows: Section 2 discusses the design, and control of the system, all details about the MPPT algorithm and variable assignments are in this section. Section 3 shows the simulation results, and Section 4 describes the hardware design as well as discusses the recorded data. Section 5 closes the paper with conclusion and recommendations.

2 Methodology

The optimum number of cells per group and converter selection has been found regarding the following issues: (i) PV cell characteristics, (ii) available micro DC–DC converters in the market, (iii) efficiency of the smart module under different shading patterns. This optimisation part of our study has been published in [23], and is briefly explained in the following subsection. Specifications of the PV cell and the chosen buck converter are shown in Tables 1 and 2. Regarding the available micro DC–DC converters in the market, the best option which was compatible with our PV cells was the one from Linear Technology: LTM4611 [30].

2.1 Least square support vector machine

For a generic study about the system, it is required to generalise the performance of the LTM4611 buck converter. To this end, the converter should be modelled with a regression function regarding its inputs (x) and outputs (y). The LS-SVM is a good method to use as it constitutes a set of related supervised learning methods which are used for both classification and regression analysis [31]. In a generic study in [23], we used the LS-SVM method to find the regression above function. The study is briefly introduced in the following two paragraphs.

A set of predetermined data from the converter datasheet are considered as the training set and is called T, where $T = \{(x_1, y_1), \ldots, (x_l, y_l)\}$, $x_j = [V_{in}(j), V_{out}(j), I_{out}(j)]^T$, and $y_j = \eta(j)$, for $j = 1, \ldots, l$ is the number of elements in data set T [30]. The training data set T is used to estimate the optimal non-linear regression function $\hat{f}$, as shown in the following equation:

$$\hat{f}(x_{\text{new}}) = \sum_{i=1}^{l} \beta K(x_{\text{new}}, x_i) + b \tag{1}$$

where K represents a so-called kernel function and for this application, the radial basis function (RBF) has been chosen as shown in the following equation:

$$K(x_{\text{new}}, x_i) = \exp\left(\frac{-\parallel x_{\text{new}} - x_i \parallel^2}{2\sigma^2}\right) \tag{2}$$

where $x_{\text{new}} = [V_{\text{in}}, V_{\text{out}}, I_{\text{out}}]^{\text{T}} \notin T$, and the design parameters β and b are obtained by solving the matrix–vector equation shown in in the following equation:

$$\begin{bmatrix} 0 & [1 \quad 1 \quad \dots \quad 1] \\ \begin{bmatrix} 1 \\ 1 \\ \vdots \\ 1 \end{bmatrix} & \left[\boldsymbol{\Omega}_{l\times l} + \left(\frac{1}{\gamma}\right)\boldsymbol{I}_{l\times l}\right] \end{bmatrix} \begin{bmatrix} b \\ \beta \end{bmatrix} = \begin{bmatrix} 0 \\ y \end{bmatrix} \tag{3}$$

Here $\boldsymbol{I}_{l\times l}$ represents the identity matrix and $\boldsymbol{\Omega}_{l\times l}$ is a $l \times l$ full matrix with computed elements from the training data as follows:

$$\boldsymbol{\Omega}_{l\times l} = \exp\left(\frac{-\parallel x_q - x_r \parallel^2}{2\sigma^2}\right), \quad q, r = 1, \dots, l \tag{4}$$

Parameters η and γ in (3) and (4) are tuning parameters, which can be calculated using different methods, such as k-fold cross-validation, leave one out cross-validation, etc. [31].

For a panel of 60 cells there are only three possible combinations of cells considering the cells and converters specification. Implementing the LS-SVM method for optimisation made us conclude that the combination of six cells per group was the optimum case [23]. Therefore, a panel of sixty cells, with individual access to each cell, was divided into ten groups of cells, and buck converters will harvest energy from all groups of the cells.

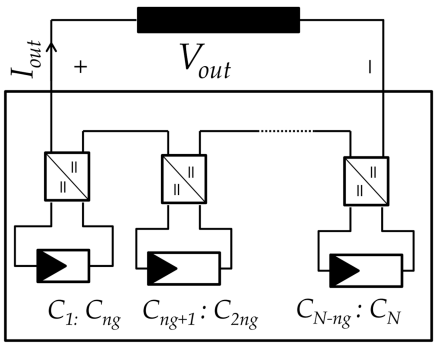

Fig. 1 *Smart module architecture*

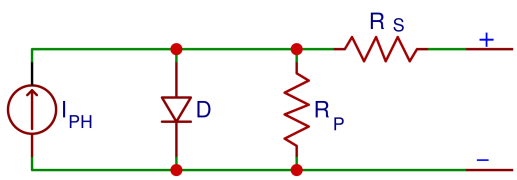

Fig. 2 *PV cell equivalent circuit*

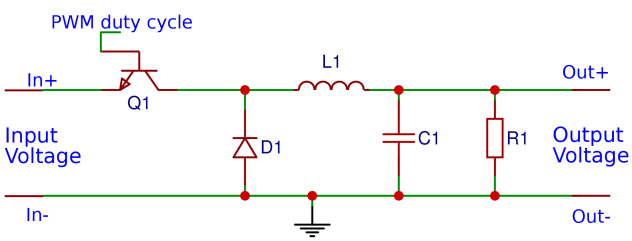

Fig. 3 *Block diagram of a basic buck converter*

In this paper, design and simulation of the hardware prototype, as well as the energy harvesting method will be discussed. The architecture of the smart panel, which is used in this study is depicted in Fig. 1. The energy harvesting method in this study is a sampling-based MPPT algorithm, and will be discussed in detail in this section. Moreover, the electronics circuits required for this study are designed and prepared by us from scratch.

2.2 Architecture

Fig. 1 shows the architecture of the smart panel. The total number of cells in the module is N and calculated as $N = N_G \times n_g$, where N_G is the number of groups in a module and n_g is the number of cells in each group. The micro-converter, for each group, is individually controlled via duty cycle $D_i, i \in [1, N_G]$, which is computed via the SM-MPPT algorithm. As mentioned above, the optimum values for N_G and n_g have been calculated as $N_G = 10$ and $n_g = 6$ [23]. Therefore, as the same architecture will be used for the hardware design, we followed the same numbers in this study as well.

2.3 PV cell model

A PV cell is modelled with a current source, I_{PH}, in parallel with a diode, D; R_{P} and R_{S} are a resistance in parallel and series with that combination, respectively. More accurate models contain two or three diodes [32]. The equivalent circuit of the one-diode model is displayed in Fig. 2

$$I_{\text{PV}} = I_{\text{PH}} - I_D - I_{R_{\text{P}}} \tag{5}$$

$$I_{\text{PV}} = I_{\text{PH}} - I_{\text{s}}\left(\exp\left(\frac{V_{\text{PV}} + IR_{\text{S}}}{mV_{\text{T}}}\right) - 1\right) - \frac{V_{\text{PV}} + IR_{\text{S}}}{R_{\text{P}}} \tag{6}$$

$$V_T = \frac{N_s K_b T}{q} \tag{7}$$

where I_{PH} and I_{s} are the photon and saturation current of PV module, respectively, K_{b} is the Boltzmann constant, m is the diode ideality factor, T is the reference temperature (K), q is the electron charge, and N_{s} is the number of cells connected in series. Due to the small voltage level of PV cells, it is necessary to connect them in series to boost up the voltage level.

2.4 Buck converter model

A block diagram of a basic buck converter is depicted in Fig. 3. The output voltage of this converter is computed as

$$V_{\text{out}} = d \times V_{\text{in}}, \quad d \in [0, 1] \tag{8}$$

where d is the duty cycle and therefore, $V_{\text{out}} \leq V_{\text{in}}$.

The converter is modelled using the state-space averaging method [33]. Therefore, the converter can be described by a single equation approximately over a number of switching cycles. The equation includes both the independent voltages and currents and also the duty cycle ratio. State equations are derived considering the on/off time of the switch Q_1 and diode D_1 as follows:

$$\text{if} \begin{cases} Q_1\text{: on} \Rightarrow \dot{x}(t) = \boldsymbol{A}_1\boldsymbol{x}(t) + \boldsymbol{B}_1 u(t) \\ Q_1\text{: off} \Rightarrow \dot{x}(t) = \boldsymbol{A}_2\boldsymbol{x}(t) + \boldsymbol{B}_2 u(t) \end{cases} \tag{9}$$

where $\boldsymbol{x}(t)$ is state variable vector and $\boldsymbol{A}_i, \boldsymbol{B}_i, i \in [1, 2]$ are system matrices and $u(t)$ is the system input. The general state-space model of the system is calculated as

$$\begin{cases} \dot{x}(t) = A\boldsymbol{x}(t) + Bu(t) \\ y(t) = C\boldsymbol{x}(t) + Du(t) \end{cases} \tag{10}$$

where A and B are defined as follows:

$$\begin{cases} A = dA_1 + (1-d)A_2 \\ B = dB_1 + (1-d)B_2 \end{cases} \tag{11}$$

Considering inductor current (i_L) and capacitor voltage (V_c) describing x like $x = [i_L\ V_c]^T$, $y(t) = [0\ 1]x(t)$ and applying Kirchhoff's laws we will have matrices for state-space model of the system in the following equation:

$$A = \begin{bmatrix} 0 & \frac{-1}{L_1} \\ \frac{1}{C_1} & \frac{-1}{R_1 C_1} \end{bmatrix}, \quad B = \begin{bmatrix} \frac{d}{L_1} \\ 0 \end{bmatrix}, \quad C = [0\ 1], \quad D = 0 \tag{12}$$

The transfer function of the buck converter is defined as linear mapping of the Laplace transform of input $U(s) = \mathscr{L}\{u(t)\}$ to the Laplace transform of output $Y(s) = \mathscr{L}\{y(t)\}$ and is derived in the following equations:

$$G(s) \times U(s) = Y(s) \tag{13}$$

$$G(s) = C(sI - A)^{-1}B + D \tag{14}$$

Regarding the built in inductor and capacitor values in LTM4611 and the possible external capacitor for the system mentioned in [30], the transfer function for the system, in the s-plane, is derived as stated in the following equation:

$$G(s) = \frac{d \times 5 \times 10^{13}}{s^2 + 5 \times 10^5\,\mathrm{s} + 5 \times 10^{13}} \tag{15}$$

The settling time for a linear system to step changes in the input can be approximated by the following formula:

$$t_s = 4/\sigma \tag{16}$$

where σ is the absolute of the real value of the most dominant pair of the complex conjugate poles. Regarding the above-mentioned calculations, in this system the settling time for the buck converter itself is 16 µs. However, as we would like to implement the chip and noting that the chip consists besides the buck converter also some other units without enough technical information to model, the settling time for the full chip needs to be investigated. In the following subsection, LTSpice software is used to investigate the exact settling time for the chip which is expected to be longer the buck converter settling time.

2.5 SM-MPPT algorithm

In this study, a SM-MPPT algorithm as a sampling-based method is proposed. The sampling frequency (f_{sp}) in this algorithm is related to the settling time of the LTM4611. As mentioned before, LTSpice software [34] is implemented to study the step response of LTM4611 with different output voltage levels, using micro-converter data from its datasheet [30].

Fig. 4 shows the step responses to the input voltage $V_{in} = 3.2$ V with different duty cycles that cause different output voltage levels. The blue points in the figure indicate when the dynamic system reached the steady-state condition. With linear curve fitting technique, the function for the black line in the figure is computed with the following equation $V_{out} = (3.8 \times 10^4)t + 26$. By solving this equation, the maximum value for settling time is $t_{s_{max}} = 0.6842$ ms. Thus, the minimum value for the sampling frequency, $f_{sp_{min}}$, can be calculated from $f_{sp_{min}} = 1/t_{sp_{max}}$ where $t_{sp_{max}}$ is the maximum value for the sampling time and we find $t_{sp_{max}} = t_{s_{max}} = 0.6842$ ms; as a result, in the SM-MPPT algorithm f_{sp} is set to $f_{sp} \leq 1.4$ kHz which is compatible with the chosen converter, as the sampling frequency is specified as 835 Hz (Table 2).

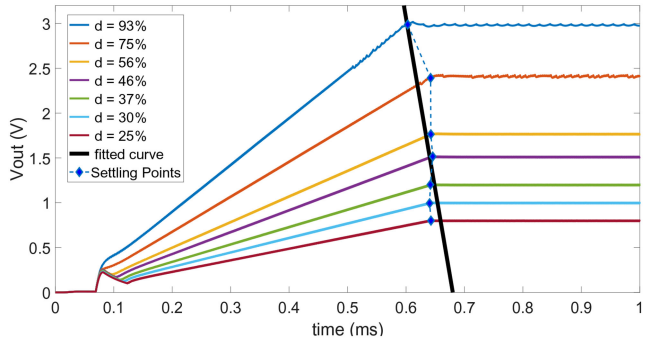

Fig. 4 *Step response of LTM4611 with $V_{in} = 3.2$ V*

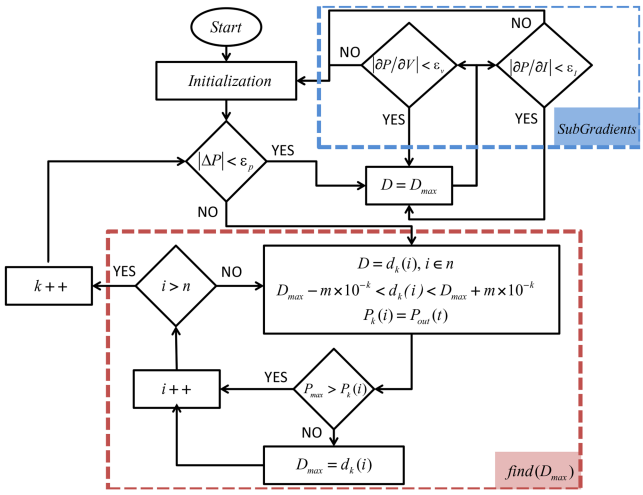

Fig. 5 *Sweep method MPPT algorithm flowchart*

The SM-MPPT algorithm is based on a high-frequency sampling method and by sweeping the duty cycle over the entire search space, the optimum operating point can be found. As shown in Fig. 5, the algorithm starts its work with initialisation and continues with two main functions of $find(D_{max})$ and *SubGradients*. The $find(D_{max})$ function is implemented to find the optimum duty cycle for the ongoing condition in one iteration. Each iteration consists of $n \in \mathbb{N}$ samples. Two other coefficients k and m are used to adjust the duty cycle precision; in this simulation, with $n = 10$, $m = 5$ and $k = 2$. Additionally, the sampling frequency as mentioned before depends on the converter settling time and is equal to 1.4 kHz.

The *SubGradients* function is implemented to check if the operating point is moved. This may occur because of either an irradiation or temperature change. Two sub-gradients $\partial P/\partial V$ and $\partial P/\partial I$, as stated in (17) and (18) are used to indicate if the operating point moves

$$\frac{\partial P}{\partial V} = \frac{P_{t+t_{sp}} - P_t}{V_{t+t_{sp}} - V_t} \tag{17}$$

$$\frac{\partial P}{\partial I} = \frac{P_{t+t_{sp}} - P_t}{I_{t+t_{sp}} - I_t} \tag{18}$$

where $\Gamma_j, \Gamma \in (V, I, P)$ is the output variable at time j and V, I, and P are voltage, current and power, respectively; t_{sp} is the sampling time and equal to $t_{sp} = 1/f_{sp}$. If the *SubGradients* function recognises that the operating point is moved, the algorithm restarts from the initialisation step. Duty cycle (D) as the control signal for micro-converter, is generated n times in each iteration

$$D = d_k(i), i \in n \tag{19}$$

The output power from the PV cells group is compared with previous output powers in the iteration. The maximum power and its matching duty cycle are recorded as P_{max} and D_{max}, respectively,

$$P_k(i) = P_{out}(t) \tag{20}$$

3 Simulations

The smart module has been simulated in MATLAB Simulink environment for a dynamically changing shading condition, which is caused by a moving object casting a shadow on the smart module. The PV cell and buck converter models are implemented in the simulation as discussed in Section 2.

3.1 Results and discussions

It is assumed that the object moves in three time windows within 0.2 s, and the performance of smart panel is studied in these time windows (TWs). Fig. 6 shows the position of shadow in each TW, it shows the position of shading the module. As shown in this figure, a smart module consists of ten groups of six cells, numbered 1 to 10, and the conventional module consists of three series strings, shown in red with PS_i, $i \in [1, 3]$. Fig. 7 depicts the output power from both modules. The darker shades on PS_1 and PS_2 is the reason why these two strings are bypassed with the BPDs and the only effective string is PS_3 in the depicted PSC.

In this condition, we assume that global horizontal irradiance is $\text{GHI} = 1000\,\text{W/m}^2$ and diffuse irradiance is equal to $G_{\text{dif}} = 700\,\text{W/m}^2$. The irradiance over the cell is calculated with (21) [35]

$$G_c = (F_{\text{shaded}} \times G_{\text{dif}}) + (F_{\text{unshaded}} \times G_{\text{GHI}}) \tag{21}$$

where F_{shaded} and F_{unshaded} are shaded and unshaded fractions of the cell area, respectively. Also, the cell with the lowest amount of irradiance determines the output from each group, in the smart module, or string, in the conventional module. A brief comparison between the conventional (C) and the smart (S) module in this test is tabulated in Table 3. $P_{\text{Out}_S}(W)$ and $P_{\text{Out}_C}(W)$ indicate the output power extracted from the smart and conventional module, respectively. It can be concluded that the smart module topology extracts 3.5 times more energy, on average, from the same cells, compared with the conventional series string module topology.

Fig. 8 depicts the PV cell-groups output power, voltage and generated duty cycles for DC–DC micro-converters for all ten groups in the three TWs, respectively. The chain of events in the simulation results of this case study is as follows:

At $t \in (0, 0.06)$s, the SM-MPPT algorithm finds the best duty cycle for all ten groups. Results show duty cycles, output power, and converter output voltage are the same for the unshaded groups of cells with the same irradiation level.

At $t \in (0.06, 0.12)$s, the change in the shading pattern affects the irradiation level on four groups. SM-MPPT recognised the change in the operating point of four groups and found new MPPs for them. Also, it did not change the duty cycle for the unshaded groups.

At $t \in (0.12, 0.2)$s, the change in the shading pattern affects the irradiation level only on three groups and the duty cycle changed only for these groups.

Moreover, the shaded groups perform at their optimum power points, and maximum power is harvested from all ten groups in all three different shading patterns. Because the converters are connected in series, the converter output voltage is changed in case of a change in operating point to continue supplying the same output current.

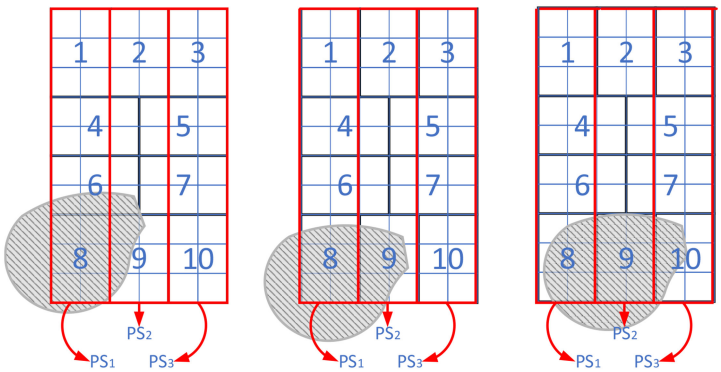

Fig. 6 *Shadow position for the three time windows*

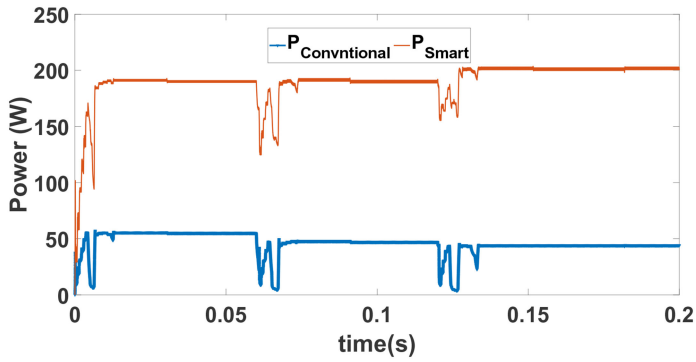

Fig. 7 *Output power of the smart (orange line) and conventional (blue line) module*

Table 3 Smart and Conventional module performance in the partial shading conditions for the three time windows of Fig. 6

TW	F_{shaded}, %	F_{unshaded}, %	P_{Out_S}, W	P_{Out_C}, W
1	15	85	190.1	55.3
2	14	86	190.6	46.6
3	18	82	201.2	44.3

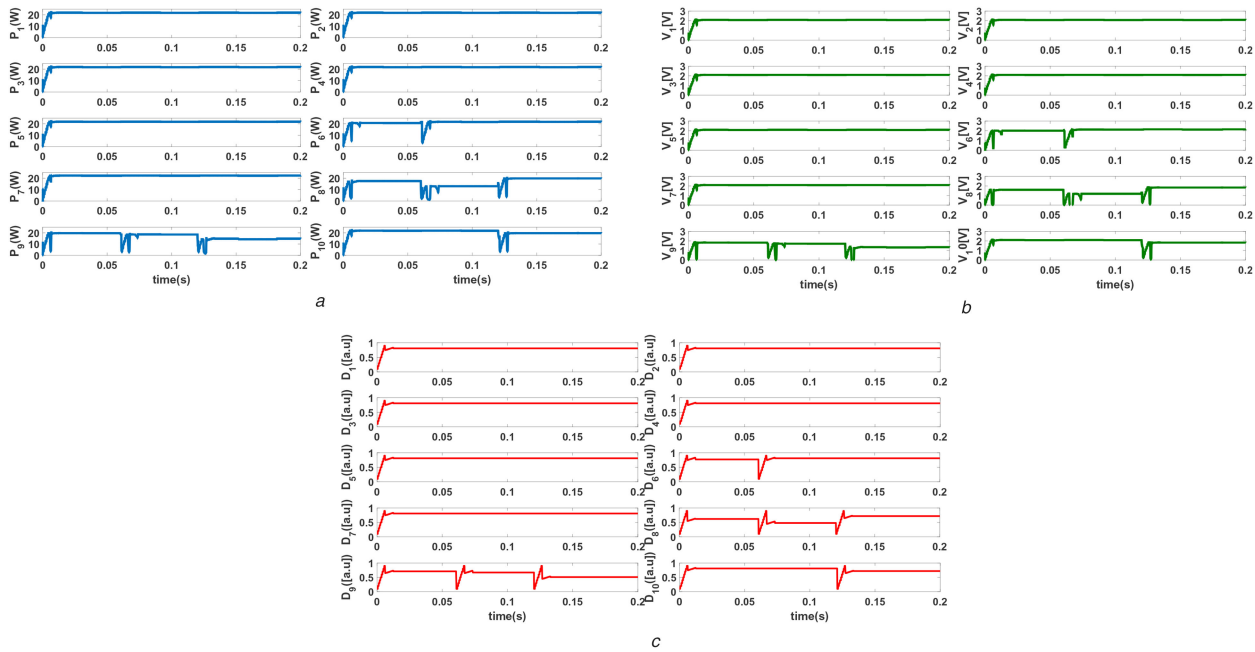

Fig. 8 *Output from all ten group of cells*
(a) Power, ***(b)*** Voltage, ***(c)*** Duty cycles

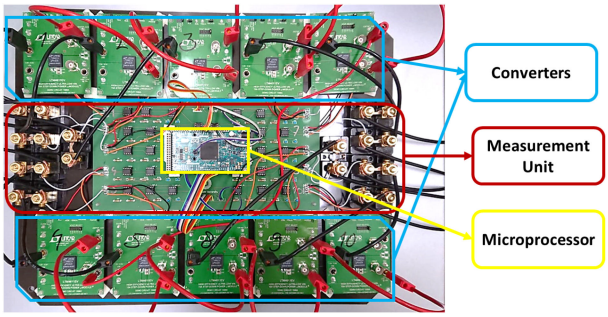

Fig. 9 *Prototype board*

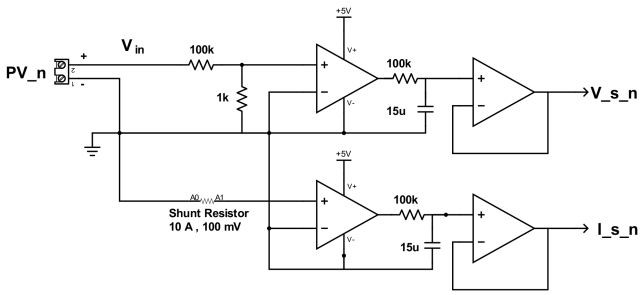

Fig. 10 *Voltage, current sensor circuit*

4 Hardware

A photograph of the developed hardware is shown in Fig. 9. The prototype board dimension is 20 × 30 cm; the prototype hardware consists of three different units:

(i) *The measurement unit:* this part of the prototype is designed to measure the voltage and current of all ten groups of the PV module, the measured values are transferred to the microprocessor.
(ii) *The microprocessor:* this unit is used to process the transferred data from the measurement unit, and to generate the reference signals to control all ten converters.
(iii) *Buck converter:* each group of cells is equipped with a DC–DC buck converter, which is controlled with a control signal generated with the MPPT algorithm explained above.

In the following, all the units mentioned above will be discussed individually in different subsections.

4.1 Measurement unit

This unit consists of ten sub-units that measure data: each sub-unit measures the output voltage and output current from one group of cells. Fig. 10 illustrates the schematics of a sub-unit. A voltage divider with a combination of $R_1 = 100\,\text{k}\Omega$ and $R_2 = 1\,\text{k}\Omega$ is used for sensing the voltage and a shunt resistor RSA-10-10 10 A/100 mV is implemented as the current sensor. Shunt resistors are much more robust compared to a Hall effect current sensor and also generate much lower noise while sensing, which is the reason why an RSA is chosen for generating the current value signal.

Fig. 10 depicts a two-level signal processing circuit where both sensed signals are first amplified, and then the noise is filtered out for preparation of the signal to the microprocessor. The Integrated Circuit (IC) AD626ANZ is a Single-Supply Differential Amplifier [36], and is implemented in each sub-unit in the two-level circuit.

4.2 Microprocessor

A 32-bit Acorn RISC Machine (ARM) core microcontroller is used for data analysis and MPPT algorithm implementation for all groups. Inputs of the controller are voltage and current signals, and the main outputs are control signals for the DC–DC converters.

There are altogether 20 signals to be read and processed in the microprocessor, but the aforementioned microcontroller has only 12 analogue input pins. To mitigate this issue, one multiplexer (MUX CD74HC4051E [37]) is implemented per five signals in the circuit to read the signals from each group and write the respective signal to the microcontroller input gates. The MUX is controlled via a data selector signal which is generates in the ARM. Once the signal is sent, the ARM reads the signals, processes them and calibrates the exact value of voltage and current. Then, it implements the calibrated data in the SM-MPPT algorithm. Finally, converter control signals will be written to the assigned digital outputs. These control signals are generated for the converter control and will be discussed in the next subsection in greater detail.

4.3 Buck converter

As discussed in [23] for this study the LTM4611 is selected from the available DC–DC buck converters in the market. In this prototype a demo board for this converter is implemented. In this demo board, the converter could be controlled via its duty cycle, and the duty cycle itself is a function of a feedback resistor (FBR). Therefore, a digital potentiometer is implemented as an interface to

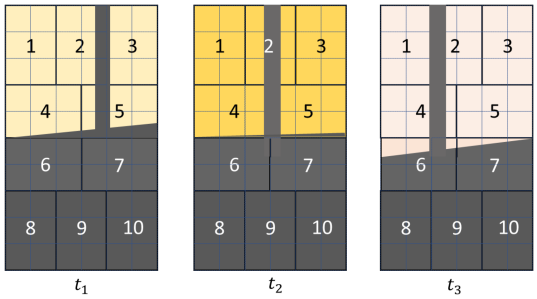

Fig. 11 *Shades move in three time windows*

Fig. 12 *Smart panel under partial shading conditions*

control the duty cycle and as a result to control the converter outputs. In this study, the MCP4161-502EP is used for this purpose, which is connected in series with a 20 kΩ resistor could change the FBR in the range of [20, 25] kΩ, while the input signal of that could change from 0 to 255. This range for FBR is calculated from converter specifications where it could perform correctly regarding the range of its supplied voltage [30].

4.4 Practical test results and discussions

To investigate the feasibility of the smart module, we tested the module under a partial shading condition at the PV lab at Utrecht University campus, and record data for about 1 h. In Fig. 11, the variation of shadings is roughly depicted in three TWs of $t_1 \in [0, 20]$ min, $t_2 \in [20, 40]$ min, and $t_3 \in [40, 60]$ min over the panel surface during the data logging. The maximum irradiation level measured on the panel surface within the one-hour data logging duration is 350 W/m^2, this value is measured with a pyranometer, which was located on the top of the module. It should be taken into consideration that Fig. 11 shows only the starting point of the TWs, while the solid and pole shadows move during each TW to reach the next frame.

In this figure, only the pole and solid obstacles' shades are shown, and shades from adjacent tree leaves which moved randomly and rapidly are not depicted. These particular causes of shades can be seen in Fig. 12, where the panel at six different shading conditions is depicted. The photos could give some idea about how the shadings move over the panel surface. The location of the panel is selected under a very random shading condition to investigate the performance of the smart panel under very random and fast-changing conditions. Fig. 13 shows the output power from each group of cells in real time. Figs. 14 and 15 depict the output for both voltage and current from each group of cells, respectively. These figures illustrate the effect of shading and the performance of the SM-MPPT algorithm. Output power shows how the MPPT algorithm extracts maximum power from each group of cell; output voltage illustrates how the duty cycle, as the control signal, controls the voltage and output current shows how the varying irradiation changes the output current. In following, regarding the figures above, the performance of a smart panel during each TW will be discussed in details.

The chain of events for this practical testing will be discussed in the following paragraphs. We will use the following three abbreviations to identify the type of shading that is affecting the module: (i) pole shade (PSh), (ii) solid obstacle shade (SOSh), (iii) tree leaves shades (TLSh).

At $t_1 \in [0, 20]$ min: In this time, window nor group G_1 covered with PSh neither SOSh, but sometimes during this TW this group is covered with TLSh, for instance at t_1 between 8 and 11 min. Groups G_2, G_3 and G_5 are under PSh. However, the group G_5 also is covered with SOSh, and also G_2 and G_3 are covered with TLSh randomly. G_4 is partially covered with SOSh and the rest of groups are covered completely with this shadow. G_4 and G_5 are rarely covered with TLSh in this TW.

Table 4 shows the average output power from each group of cells, from which G_4 extracted the maximum amount of power during this TW and its average power is 2.14 W. Other best groups are G_5 and G_1, with 1.87 and 1.27 W output power. Fig. 13 shows how the output power varies from the first moment till the end of this TW. For example, G_4 starts with very low output power and as

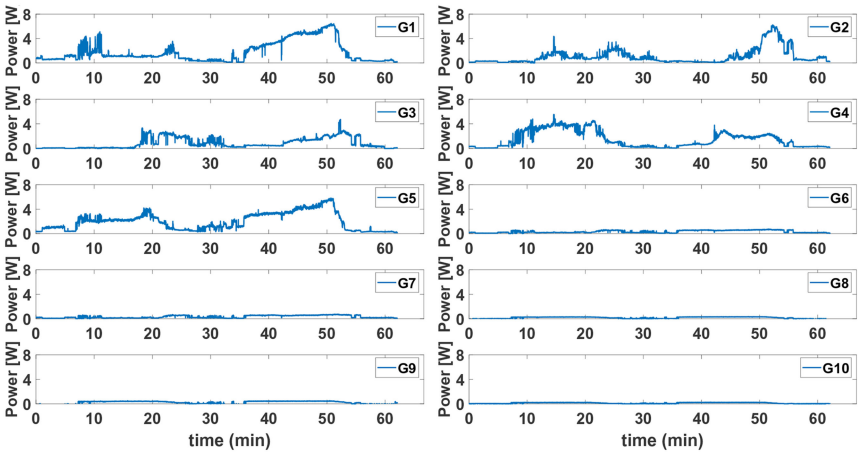

Fig. 13 *Output power from the smart panel*

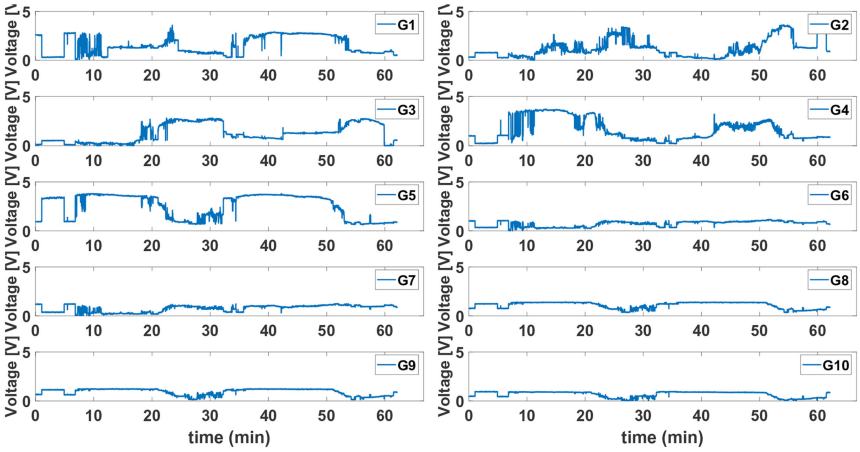

Fig. 14 *Output voltage from the smart panel*

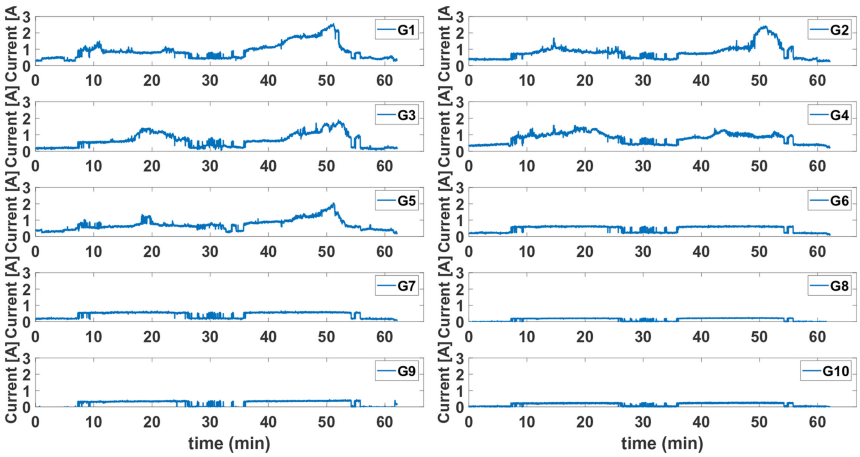

Fig. 15 *Output current from the smart panel*

a result of the movement of SOSh the output power from this group increased remarkably. The average output power from the whole module in this TW is 7.13 W, however, for a conventional PV module the output power in this condition would be related to the output from the most shaded groups namely G_8, G_9, and G_{10} and would have been almost 1.75 W.

At $t_2 \in [20, 40]$ min: Groups G_1 and G_3 in this TW are only under the coverage of TLSh. The PSh in this TW covers three groups: G_2, G_4, and G_5. This shade moves during this TW towards the left. The rest of the groups are under SOSh. However, this shade moves during this TW downward.

As tabulated in Table 4, G_5 extracted the maximum average power within this period, and that is because PSh relocated from this group during this period. The effect of PSh and TLSh is clearly shown on the group G_4 with a 60% decrease in its output power compared to the previous TW. G_1 and G_3 are second and third respect to maximum output power, as these groups are not covered with dark PSh and SOSh. The overall average output power from the smart module in this TW is 6.67 W. Regarding the output power/current from groups under dark shades it is clear that total average output within this TW for a conventional panel would be almost 1.74 W.

At $t_3 \in [40, 60]$ min: Groups G_1, G_3 and G_5 in this TW are only under coverage of TLSh. Groups $G_i, i \in (2, 4, 6)$ are covered partially with PSh in this TW. Group G_7 at the beginning of this TW comes out partially from the SOSh. The rest of the groups are under dark SOSh, and similar to the previous TW, this shade moves during this TW downward and PSh moves to the left.

Table 4 Average power in each TW from each group of cells

Group	TW	G_1	G_2	G_3	G_4	G_5
average power, W	t_1	1.2688	0.6373	0.3374	2.1413	1.8710
	t_2	1.2737	0.7849	1.0058	0.8542	1.6238
	t_3	2.8691	1.7141	1.2301	1.3551	2.4370

Group	TW	G_6	G_7	G_8	G_9	G_{10}
average power, W	t_1	0.1958	0.1628	0.1701	0.2326	0.1307
	t_2	0.4452	0.4415	0.1770	0.2526	0.1172
	t_3	0.3611	0.3528	0.1432	0.1908	0.0968

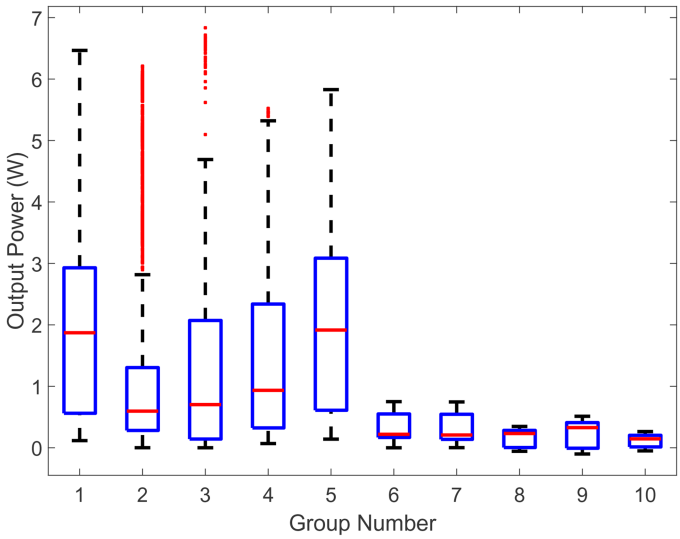

Fig. 16 *Output power from groups*

Table 5 Average output power from both simulation and hardware experiment

Panel	Power, W		Ratio%, a.u.	
	Simulation[a]	Prototype[a]	Simulation	Prototype
smart panel	193.96	8.31	398%	508%
conventional panel	48.73	1.63		

[a]Ambient condition is different in simulation and prototype testing.

Table 4 shows the maximum average extracted power is from the group G_1 and followed by the group G_5. These two groups are only covered with TLSh; it is clearly shown in Fig. 12 and also tabulated in Table 4 that group G_3 is covered with lots of TLSh, and that is due to the change in sun tilt angle, which changes the TLSh patterns. Comparing groups G_1 and G_2 in Fig. 13 shows that once the PSh moves to the left the output power from G_2 increases a lot, but output power from group G_1 decreases, which is the effect of PSh. Average output power for the whole smart panel within the last TW is 11.1 W. The overall average increased 167% compared to the previous TW. The conventional panel in this TW extracts 1.38 W.

Fig. 16 shows the output power from different groups in the smart module. This figure depicts how the shading could affect the output power from a group of cells with similar characteristics and different shading patterns. $G_6 - G_{10}$ are mainly under SOSh, and that is the reason for their very low output power. This figure shows G_2 and G_3 have experience of being under very dynamic TLSh.

Table 5 tabulates a very brief conclusion on how two typologies of smart and conventional panels performed under PSC for both simulation and hardware experiments.

From the results presented here, we can state that the average output power in the smart module is higher than the expected average power from a conventional module with three BPDs. Regarding these values, the smart module extracted on average 8.31 W in a very restricted shading condition with three different shade types and also maximum irradiation of 350 W/m^2. However, considering the outputs from groups with the most shaded condition a conventional panel in this testing condition could generate only about 1.63 W. It can be concluded that both in simulation and prototype testing condition, smart module performed much better compared to the conventional panel. Tabulated in Table 5 smart module performed almost 508% better than a conventional module with BPDs.

5 Conclusion

In this paper, a smart module using a micro-buck converter is proposed. The module is designed such that even at low irradiation due to shading optimal power is generated. A sample-based MPPT algorithm with two functions is introduced in this paper. To investigate the functionality of the design, the MATLAB-SIMULINK environment is used. Simulation tests showed the smart panel could follow fast changes (<0.2 s) in shading patterns very well.

As a proof of concept, a hardware prototype for this module has been built. This prototype is tested under partial shading conditions with three different shade types. Testing has been done for this module for about 1 h, and the logged data is used for analysis in

this work. The outcomes from hardware testing showed that the smart module is functioning well and that it could extract about 5.1 times more power compared to a conventional module with three BPDs in the testing above conditions. Future work will include longer outdoor tests to assess the benefits at longer timescales.

6 Acknowledgments

The authors gratefully acknowledge fruitful discussions with Rudi Jonkman and Robert van der Sanden (Heliox), Lenneke Sloof (ECN). This work was partly financially supported by the Netherlands Enterprise Agency (RVO) within the framework of the Dutch Topsector Energy (project Scalable Shade Tolerant Modules, SSTM).

7 References

[1] The International Energy Agency (IEA): '2016 SNAPSHOT OF GLOBAL PHOTOVOLTAIC MARKETS'

[2] The International Energy Agency (IEA): '2018 SNAPSHOT OF GLOBAL PHOTOVOLTAIC MARKETS'

[3] Moraitis, P., Kausika, B, Nortier, N., *et al.*: 'Urban environment and solar PV performance: the case of the Netherlands', *Energies*, 2018, **11**, (6), p. 1333

[4] Salas, V., Olias, E., Barrado, A., *et al.*: 'Review of the maximum power point tracking algorithms for stand-alone photovoltaic systems', *Sol. Energy Mater. Sol. Cells*, 2006, **90**, (11), pp. 1555–1578

[5] Bidram, A., Davoudi, A., Balog, R.S.: 'Control and circuit techniques to mitigate partial shading effects in photovoltaic arrays', *IEEE J. Photovoltaics*, 2012, **2**, (4), pp. 532–546

[6] Olalla, C., Clement, D., Rodriguez, M., *et al.*: 'Architectures and control of submodule integrated DC–DC converters for photovoltaic applications', *IEEE Trans. Power Electron.*, 2013, **28**, (6), pp. 2980–2997

[7] Mirhassani, S.M., Golroodbari, S.Z.M., Golroodbari, S.M.M., *et al.*: 'An improved particle swarm optimization based maximum power point tracking strategy with variable sampling time', *Int. J. Electr. Power Energy Syst.*, 2015, **64**, pp. 761–770

[8] Velasco-Quesada, G., Guinjoan-Gispert, F., Pique-Lopez, R., *et al.*: 'Electrical PV array reconfiguration strategy for energy extraction improvement in grid-connected PV systems', *IEEE Trans. Ind. Electron.*, 2009, **56**, (11), pp. 4319–4331

[9] Takashima, T., Tanaka, T., Amano, M., *et al.*: 'Maximum output control of photovoltaic (PV) array'. Collection of Technical Papers. 35th Intersociety Energy Conversion Engineering Conf. and Exhibit (IECEC) (Cat. No.00CH37022), Las Vegas, NV, USA, July 2000, vol. 1, pp. 380–383

[10] Schoeman, J.J., van Wyk, J.D.: 'A simplified maximal power controller for terrestrial photovoltaic panel arrays'. 1982 IEEE Power Electronics Specialists Conf., Cambridge, MA, USA, June 1982, pp. 361–367

[11] Mirbagheri, S.Z., Mekhilef, S., Mirhassani, S.M.: 'MPPT with Inc.Cond method using conventional interleaved boost converter', *Energy Procedia*, 2013, **42**, pp. 24–32

[12] Safari, A., Mekhilef, S.: 'Simulation and hardware implementation of incremental conductance MPPT with direct control method using Cuk converter', *IEEE Trans. Ind. Electron.*, 2011, **58**, (4), pp. 1154–1161

[13] Radjai, T., Rahmani, L., Mekhilef, S., *et al.*: 'Implementation of a modified incremental conductance MPPT algorithm with direct control based on a fuzzy duty cycle change estimator using dSPACE', *Sol. Energy*, 2014, **110**, pp. 325–337

[14] Ramli, M.A.M., Twaha, S., Ishaque, K., *et al.*: 'A review on maximum power point tracking for photovoltaic systems with and without shading conditions', *Renew. Sustain. Energy Rev.*, 2017, **67**, pp. 144–159

[15] Mirbagheri, S.Z., Aldeen, M., Saha, S.: 'A PSO-based MPPT re-initialised by incremental conductance method for a standalone PV system'. 2015 23rd Mediterranean Conf. on Control and Automation, MED 2015 – Conf. Proc., Torremolinos, Spain, 2015

[16] Aouchiche, N., Aitcheikh, M.S., Becherif, M., *et al.*: 'AI-based global MPPT for partial shaded grid connected PV plant via MFO approach', *Sol. Energy*, 2018, **171**, pp. 593–603

[17] Sher, H.A., Murtaza, A.F., Noman, A., *et al.*: 'A new sensorless hybrid MPPT algorithm based on fractional short-circuit current measurement and P&O MPPT', *IEEE Trans. Sustain. Energy*, 2015, **6**, (4), pp. 1426–1434

[18] Aurilio, G., Balato, M., Graditi, G., *et al.*: 'Fast hybrid MPPT technique for photovoltaic applications: numerical and experimental validation', *Adv. Power Electron.*, 2014, **2014**, Article ID 125918

[19] Pannebakker, B.B., de Waal, A.C., van Sark, W.G.J.H.M.: 'Photovoltaics in the shade: one bypass diode per solar cell revisited', *Prog. Photovolt., Res. Appl.*, 2017, **25**, (10), pp. 836–849

[20] Tey, K.S., Mekhilef, S.: 'Modified incremental conductance algorithm for photovoltaic system under partial shading conditions and load variation', *IEEE Trans. Ind. Electron.*, 2014, **61**, (10), pp. 5384–5392

[21] Soon, T.K., Mekhilef, S.: 'A fast-converging MPPT technique for photovoltaic system under fast-varying solar irradiation and load resistance', *IEEE Trans. Ind. Inf.*, 2015, **11**, (1), pp. 176–186

[22] Reisi, A.R., Moradi, M.H., Jamasb, S.: 'Classification and comparison of maximum power point tracking techniques for photovoltaic system: a review', *Renew. Sustain. Energy Rev.*, 2013, **19**, pp. 433–443

[23] Mirbagheri Golroodbari, S., de Waal, A., van Sark, W.: 'Improvement of shade resilience in photovoltaic modules using buck converters in a smart module architecture', *Energies*, 2018, **11**, (2), p. 250

[24] Schmidt, H., Rogalla, S., Goeldi, B., *et al.*: 'Module integrated electronics – an overview'. 25th European Photovoltaic Solar Energy Conf. and Exhibition/5th World Conf. on Photovoltaic Energy Conversion, Valencia, Spain, 6–10 September 2010, pp. 3700–3707, October 2010

[25] Lopez-Santos, O., Garcia, G., Martinez-Salamero, L., *et al.*: 'Analysis, design, and implementation of a static conductance-based MPPT method', *IEEE Trans. Power Electron.*, 2019, **34**, (2), pp. 1960–1979

[26] Dolara, A., Grimaccia, F., Mussetta, M., *et al.*: 'An evolutionary-based MPPT algorithm for photovoltaic systems under dynamic partial shading', *Appl. Sci.*, 2018, **8**, (4), p. 558

[27] Uno, M., Kukita, A.: 'Current sensorless equalization strategy for a single-switch voltage equalizer using multistacked buck–boost converters for photovoltaic modules under partial shading', *IEEE Trans. Ind. Appl.*, 2017, **53**, (1), pp. 420–429

[28] Abu Qahouq, J.A., Jiang, Y.: 'Distributed photovoltaic solar system architecture with single-power inductor single-power converter and single-sensor single maximum power point tracking controller', *IET Power Electron.*, 2014, **7**, (10), pp. 2600–2609

[29] Jiang, Y., Qahouq, J.A.A.: 'Single-sensor multi-channel maximum power point tracking controller for photovoltaic Solar Systems', *IET Power Electron.*, 2012, **5**, (8), pp. 1581–1592

[30] Linear Technology: 'LTM4611/ typical application ultralow VIN, 15A DC/DC micro module regulator'

[31] Burges, C.J.C.: 'A tutorial on support vector machines for pattern recognition', *Data Min. Knowl. Discov.*, 1998, **2**, pp. 1–43

[32] Gow, J.A., Manning, C.D.: 'Development of a photovoltaic array model for use in power-electronics simulation studies', *IEE Proc.- Electr. Power Appl.*, 1999, **146**, (2), pp. 193–200

[33] Cuk, S., Middlebrook, R.D.: 'A general unified approach to modelling switching DC-to-DC converters in discontinuous conduction mode'. 1977 IEEE Power Electronics Specialists Conf., Palo Alto, CA, USA, June 1977, pp. 36–57

[34] Analog Devices. Ltspice. 1995–2018

[35] Sinapis, K., Tzikas, C., Litjens, G., *et al.*: 'A comprehensive study on partial shading response of c-Si modules and yield modeling of string inverter and module level power electronics', *Sol. Energy*, 2016, **135**, pp. 731–741

[36] Analog Devices: 'AD626 low cost, single-supply differential amplifier'. Technical report, 2003

[37] Texas Instruments: 'CDx4HC405x, CDx4HCT405x high-speed CMOS logic analog multiplexers and demultiplexers'

8 Appendix

In this section, the schematic circuit of the whole system is presented in Fig. 17.

Fig. 18 shows the PCB designed for this schematic which is used in the prototype.

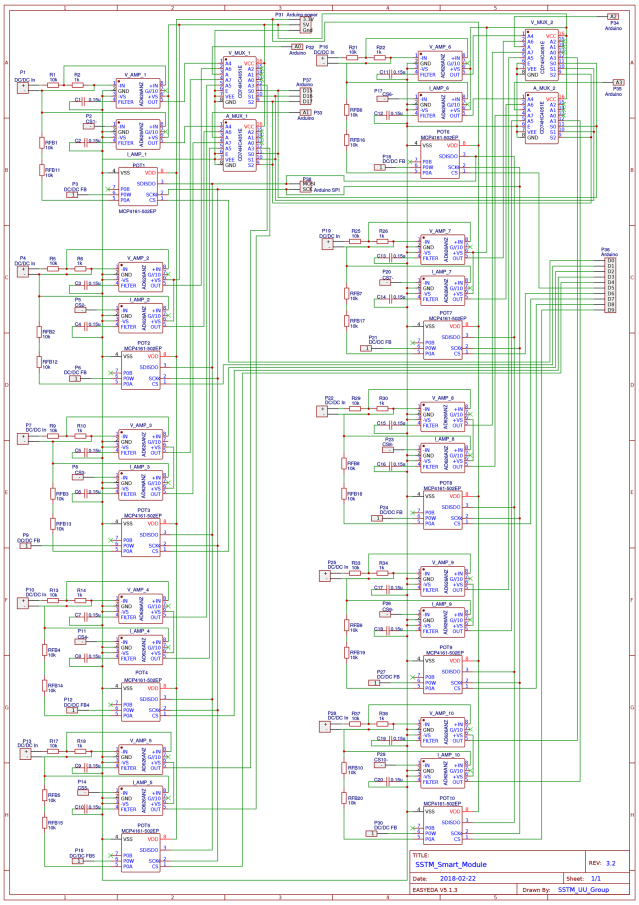

Fig. 17 *Electronics circuit schematic*

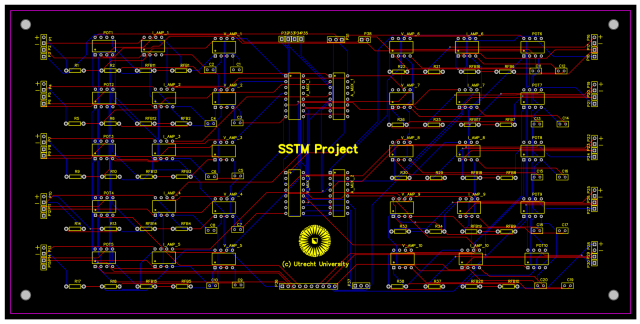

Fig. 18 *PCB layout for the electronic circuit of the smart panel*